A model for axonal propagation incorporating both radial and axial ionic transport

J. M. van Egeraat*‡ and J. P. Wikswo, Jr.*

*Living State Physics Group, Department of Physics and Astronomy, Vanderbilt University, Nashville, Tennessee 37235 USA; and
‡Department of Neurology, Faculty of Medicine, Erasmus University, 3000 DR Rotterdam, The Netherlands

ABSTRACT We present an axonal model that explicitly includes ionic diffusion in the intracellular, periaxonal, and extracellular spaces and that incorporates a Hodgkin–Huxley membrane, extended with potassium channel inactivation and active ion transport. Although ionic concentration changes may not be significant in the time course of one action potential, they are important when considering the long-term behavior (seconds to minutes) of an axon. We demonstrate this point with simulations of transected axons where ions are moving between the intra- and extracellular spaces through an opening that is sealing with time. The model predicts that sealing must occur within a critical time interval after the initial injury to prevent the entire axon from becoming permanently depolarized. This critical time interval becomes considerably shorter when active ion transport is disabled. Furthermore, the model can be used to study the effects of sodium and potassium channel inactivation; e.g., sodium inactivation must be almost complete (within 0.02%) to obtain simulation results that are realistic.

INTRODUCTION

The modeling of electrophysiological events in nerves is usually based on the assumption that the ionic concentrations are constant in both space and time. The original Hodgkin–Huxley (HH) model (1) is probably the best-known example of such a model. In this model, the Nernst potentials for the different ion species are kept constant, which means that the ratio of the intra- and extracellular ion concentrations for each ion species does not change. Some of the more recent cardiac membrane models (2) do have varying ionic concentrations but do not include axial diffusion. Although omission of axial diffusion is valid under many circumstances, there are a few interesting situations that require the modeling of the ionic concentrations as spatially and temporally dynamic quantities, notably the study of injured cells where there is free axial transport of ions between the cytoplasm and the extracellular space.

In this article we develop a model of action potentials propagating along an axon that explicitly includes the concentrations of many ion species. The axon is considered as a core conductor with a HH-like membrane with adjacent periaxonal space and Schwann cell layer separating the intra- and extracellular spaces. Ionic movement within either space is governed by the Nernst–Planck diffusion equation (3). To reflect the long-term behavior realistically, the HH membrane description is extended with additional mechanisms that affect membrane ion transport: the sodium and potassium concentration gradients across the membrane are maintained by active ion transport (4), and the potassium channel description is enhanced with inactivation (5). We also investigate the possible effects of slowly or noninactivating sodium channels that have been reported in the literature (6).

Address correspondence to Dr. John P. Wikswo, Jr., Living State Physics Group, Department of Physics and Astronomy, Vanderbilt University, P.O. Box 1807 Station B, Nashville, TN 37235.

Our interest in diffusional problems related to neurophysiology is prompted by our more general interest in the underlying mechanisms of nerve injury and repair. The most interesting cases clinically involve mammalian, myelinated nerve bundles, which are quite different from the squid giant axon that is used in this study. However, it seems prudent to study the nerve response to injury first at the single cell level before proceeding to nerve bundles. Furthermore, there is an abundance of quantitative physiological data available on the squid nervous system that can be used in our theoretical work. Also, predictions based on the model calculations can be verified in detail and most accurately with a squid experimental model.

The model application in this article is confined to the subject of long-term behavior of transected axons, but many other applications can be imagined. For example, spatial buffering (7, 8) and spreading depression (9–11) are neurophysiological phenomena that are related to diffusion as well. With these problems in mind, we devised our model to include the possibility for a restricted extracellular space, although this option will not play a major role in this report. However, future reports will explore other applications of the model presented herein.

MODELING

The one-dimensional Nernst–Planck electrodiffusion equation (3),

$$j_s = -D_s\left(\frac{\partial[s]}{\partial z} + \frac{z_s F}{RT}[s]\frac{\partial V}{\partial z}\right), \qquad (1)$$

describes how the ion flux j_s (mol/m^2 s) of species s at a given point depends on the diffusion constant D_s, the concentration $[s]$, and the potential V, all of which can be a function of the spatial coordinate z. The potential

0006-3495/93/04/1287/12 $2.00

gradient or electric field may be applied externally or it may arise from distributed electric charge in the fluid. F is the Faraday, R the gas constant, T the absolute temperature, and z_s the ion valence.

Eq. 1 leads to a useful corollary when we consider the total electric flux $J(A/m^2)$, which is the sum of the ion fluxes j_s, each weighted with F times its ion valence z_s. Throughout this article we will adopt the convention that ion fluxes are denoted with a lower case j and electric fluxes with an upper case J. After some algebra, we obtain what is essentially Ohm's law,

$$J = -\sigma\left(\frac{\partial V}{\partial z} - \frac{\partial V^{1j}}{\partial z}\right), \tag{2}$$

where the conductivity σ is given by

$$\sigma = \frac{F^2}{RT}\sum_s z_s^2 D_s[s]. \tag{3}$$

The second gradient,

$$\frac{\partial V^{1j}}{\partial z} = -\frac{RT}{F}\left(\frac{\sum_s z_s D_s \frac{\partial [s]}{\partial z}}{\sum_s z_s^2 D_s[s]}\right), \tag{4}$$

describes a source term that arises when the solution has concentration gradients of ions that do not all have the same diffusion constant. This source term is called the liquid junction potential (3, 12) because it exists most notably at the boundary between two solutions of different ion composition. In fact, the junction acts as a battery. The energy stored in the concentration battery is derived from the free energy of the unmixed solution. To obtain the potential difference across the junction, Eq. 4 can be integrated analytically under the common assumption that the concentrations vary linearly in the boundary region (3)

$$V^{1j}_{1\to 2} = -\frac{RT}{F}\frac{\sum_s z_s D_s([s]_1 - [s]_2)}{\sum_s z_s^2 D_s([s]_1 - [s]_2)} \times \ln\left(\frac{\sum_s z_s^2 D_s[s]_1}{\sum_s z_s^2 D_s[s]_2}\right). \tag{5}$$

With this equation we find that the liquid junction potential at the boundary of, for example, a 100-mM NaCl and a 100-mM KCl solution at room temperature is on the order of 4 mV. Instead of using Eq. 5, it may be easier to calculate the liquid junction potential with Eq. 4 in finite difference form. For the example given, the difference between the answers obtained is <1%.

We can now proceed to the construction of the axon model, schematically represented in Fig. 1. Although the model is one-dimensional, we will incorporate the appropriate scale factors so that it represents the three-dimensional, axisymmetric system of three concentric cylinders; the inner cylinder with radius r_i bounded by an axon membrane of negligible thickness separating the intracellular space from the second cylinder; and the periaxonal space, which is surrounded by a porous layer of Schwann cells with inner radius r_p and outer radius r_s. This axon is centered in an outer cylinder representing the extracellular space with radius r_e. The effective surface area of the Schwann cell layer that is available for radial diffusion between the periaxonal and extracellular spaces is a fraction of the total surface area of this layer, indicated with $f_{schwann}$ (13). For simplicity we will ignore axial diffusion in the Schwann cell layer. Although this approach ignores radial diffusion in the intra- and extracellular spaces, it is a good approximation for situations where the fiber length is much greater than the fiber diameter or where either space exhibits only large axial concentration gradients.

We will consider six ion species in our model: sodium (Na^+), potassium (K^+), and chloride (Cl^-) are included explicitly, whereas mobile, monovalent anions and divalent cations are each lumped together as A^- and C^{2+}, respectively. Finally, M^- represents the negatively charged heavy molecules (i.e., proteins) that are especially prevalent in the intracellular space and have a low diffusion coefficient (14).

For our numerical calculations we divided the system into finite elements for which an equivalent electric circuit can be given. As can be seen in Fig. 1, we allow voltage sources at all fluid interfaces so that we have intracellular, periaxonal, extracellular, and access liquid junction potentials U_i, U_p, U_e, and U_a, respectively. These liquid junction potentials are calculated according to Eq. 4. The intracellular, periaxonal, extracellular, and access resistors R_i, R_p, R_e and R_a, respectively, follow from Eq. 3 combined with the proper geometric factors, where we took an average of the periaxonal and extracellular concentrations for the calculation of R_a.

The only remaining part of the model description is the membrane, which is characterized by a membrane resistance R_m in series with a voltage source U_m and by a membrane capacitance C_m. So far this is similar to the HH model for squid giant axons (1), but a closer look at the combination of R_m and U_m in the inset of Fig. 1 shows some extensions. The sodium, potassium, and chloride Nernst potentials and permeabilities of the membrane are given by U_{Na}, U_K, and U_{Cl}, and g_{Na}, g_K, and g_{Cl}, respectively. The Nernst potential follows from the periaxonal and intracellular concentrations

$$U_s = \frac{RT}{z_s F}\ln\left(\frac{[s]_p}{[s]_i}\right). \tag{6}$$

In addition, we have an electrogenic ion pump that moves sodium ions out of the intracellular space and returns potassium ions instead in a 3:2 ratio (4). This pump is described by a pump conductivity g_{NaK} and a pump reversal potential U_{NaK}. In our calculations this

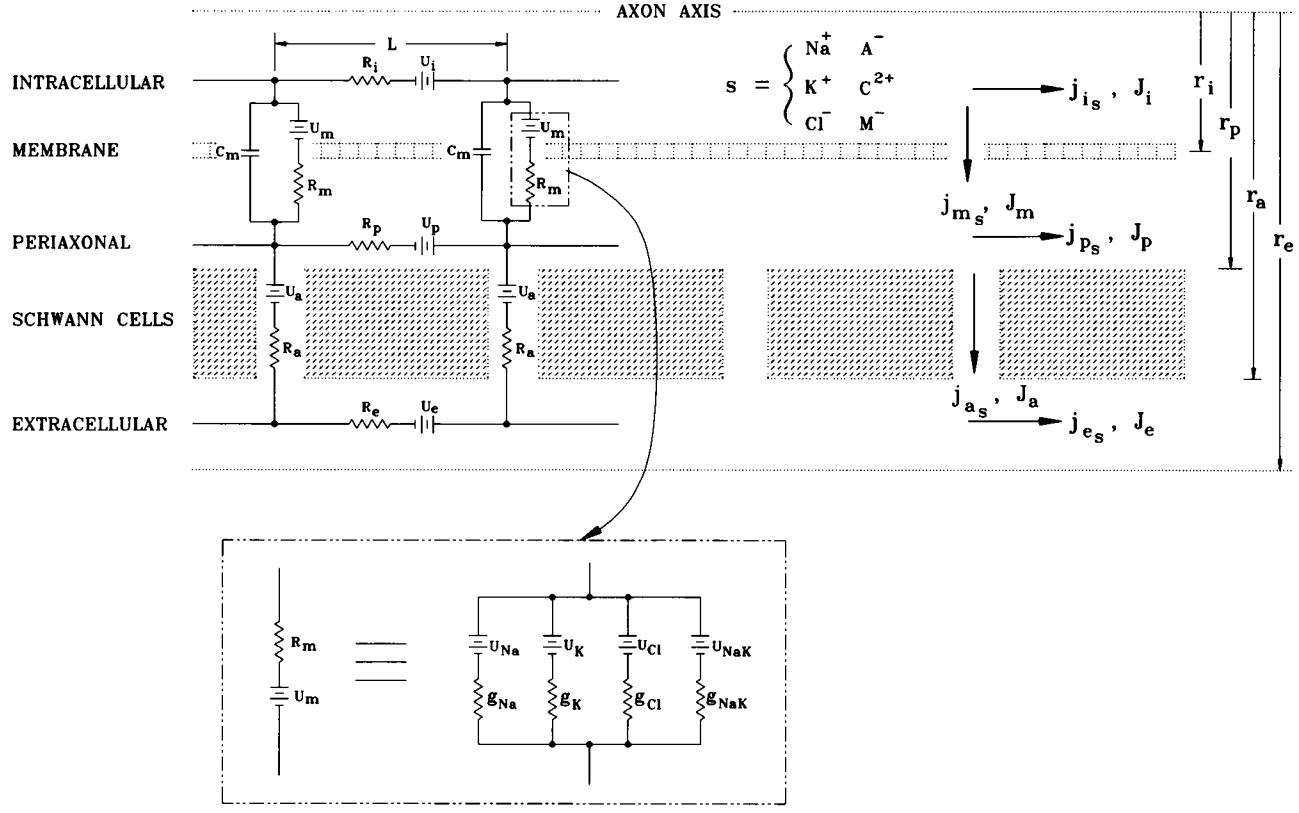

FIGURE 1 Schematic representation of the axonal model with axial and radial ion diffusion. (*Inset*) Equivalent circuit of the membrane. See text for identification of circuit components.

will be the only active transport, although there must also be some form of active chloride transport to counteract the chloride leakage. However, very little quantitative information is available on additional pump mechanisms. We will return to this point later. The membrane fluxes for sodium, potassium, and chloride are now

$$j_{m_{Na}} = \frac{1}{F}(g_{Na}m^3h(V_m - U_{Na}) + 3g_{NaK}(V_m - U_{NaK})), \quad (7)$$

$$j_{m_K} = \frac{1}{F}(g_K n_0 n^4(V_m - U_K) - 2g_{NaK}(V_m - U_{NaK})), \quad (8)$$

$$j_{m_{Cl}} = \frac{1}{F}g_{Cl}(V_m - U_{Cl}), \quad (9)$$

where m, h, and n are the familiar Hodgkin–Huxley gates, V_m is the membrane potential (the potential across C_m), and g is the maximum membrane conductivity for each ion species. The gates m, h, and n depend on the membrane potential through the rate constants as described by Hodgkin and Huxley (1). Potassium inactivation is controlled by an additional gate, n_0. Hodgkin and Huxley recorded the membrane currents over relatively short periods of time on the order of milliseconds, but further study of the potassium channel in squid giant axon (5, 15, 16) revealed that there are also slower channel kinetics that may play an important role in our model. Under normal resting conditions, n_0 will approach unity so that the potassium current follows the HH description. However, prolonged membrane depolarization on the order of seconds to minutes will make n_0 close partially (inactivation) to a value that depends sigmoidally on the membrane potential and reaches a minimum value of ~0.2 at a depolarization of −40 mV or higher. Similarly, n_0 will open only slowly after inactivation when the membrane potential returns to a normal resting value (reactivation). A detailed description of the inactivation and reactivation kinetics used in our model can be found in reference 5.

Numerical evaluation of the model consists of the following sequence. Given the ion concentrations, we can calculate the voltage sources and resistors. For the determination of the membrane voltage source and resistor (U_m and R_m), we also need the momentary state of the gates. Given the membrane potential across C_m, it is now possible to calculate the potentials at all points so that the momentary state of the model is completely known. From this we can find the ion fluxes, which with properly weighed summation give the electric flux. One timestep in the numerical evaluation is finished with a calculation of the changes in the concentrations and the membrane potential from the ion fluxes and the change of the gates from the membrane potential via the voltage-dependent rate constants (1, 5). The timestep is typi-

cally 2 μs, and the space step (the axial size of one element) is of the same order of magnitude as the intracellular radius r_i. This calculation method is of the explicit type. An implicit method (17) would have the advantage of nonconditional stability but cannot easily be applied in this case because the rate of change of the concentrations depends nonlinearly on the concentrations through the logarithmic factor in Eq. 6. This prohibits the straightforward solution of a set of linear equations as is customary in the implicit method. On a SUN 4/260 computer (Sun Microsystems, Inc., Mountain View, CA), programmed in C, a 32-node model was evaluated at a speed of 1,000 timesteps/s. An identical model on an 80486 50-MHz PC programmed in TurboPascal ran two to five times slower. When the model system is in a quasistatic state, i.e., no action potentials are propagating, the timestep can be increased several orders of magnitude, if we neglect the transient, capacitive term in the membrane current and assume that the n, m, and h gates become instantaneous functions of the membrane potential V_m. We used this method to reduce the computation time after verifying that it produced the same results as a calculation with the smaller, initial timestep used in the entire calculation.

APPLICATIONS

Transected axons without sealing

One of the interesting applications of this model is the study of the long-term behavior of an injured axon. The calculations are based on the parameters summarized in Table 1. We used a Q_{10} of 3 to obtain the rate constants at the given temperature (18). The radius r_e is chosen to be 50 times larger than r_i to approximate an infinite bath. Therefore, the extracellular potential is approximately zero at all positions, and the extracellular concentrations remain constant. In future reports we will present the case of an axon in a more restricted extracellular space.

We will begin by modeling the injury as an open connection between the axoplasm and the bath with a cross-section equal to the axon cross-section. After the transection, the proximal and distal sides of the axon are assumed to behave independently, so that we only have to model one segment. At the time of transection, the sudden depolarization elicits a single action potential, after which the membrane potential returns to a quasistatic profile indicated by the solid line in Fig. 2. The sources of the voltage profile are the Nernst potentials across the membrane and the liquid junction potentials along the cytoplasm and in the Schwann layer, all of which are determined by the concentrations. The potential of the periaxonal space with respect to the bath never exceeded 2 mV in all our injury calculations.

If we used a voltmeter to measure the potential difference 10 s after transection between the intracellular space of the element at the cut and the bath, then we would obtain a reading of −17 mV. This axial potential difference is also close to the membrane potential because the bath is large and may be treated as an equipotential, and the periaxonal potential is close to the external potential. The current entering the axon through the opening, however, is not simply the product of this potential difference and the intracellular conductance between this element and the bath (refer to Eq. 2), because there exists a 12-mV liquid junction potential at the interface with the polarity such that the "negative battery pole" is connected to the intracellular space. Therefore, the effective potential difference that must be used to calculate the current is only $-17 + 12 = -5$ mV. The sign of the liquid junction potential is such that it actually slows down the depolarization by reducing the effective voltage gradient. This demonstrates that a conventional calculation that does not include the concentration gradients will make a considerable error in determining the electric current entering the axon.

As time progresses, more of the axon will become depolarized, as shown by the broken and dotted lines in Fig. 2. This slow depolarization spreads at a velocity of ~2 μm/s, as measured between half-maximum points of the voltage profiles for 1.0, 2.5, and 5.0 ks. A low propagation velocity of 2 μm/s cannot be observed in models that solely take into account the electric quantities, since only the relatively slow ionic diffusion can explain effects that take place on such a long timescale.

The intracellular concentration profiles for all six ions are given in Fig. 3, *a–f*. The concentrations change as a result of axial and membrane ion fluxes (Fig. 3, *g–l*). The plateau in the later sodium concentration profiles is created by an increased sodium membrane flux in that region (Fig. 3 *j*). The anion concentration shows a slight downward peak in the later concentration profiles. This demonstrates that the diffusion depends on both the concentration gradient and the voltage gradient. In the region with a steep voltage gradient, the anions move faster toward the cut than would be expected based on the concentration gradient alone, thereby leaving behind an area with a relative anion depletion. The heavy ion concentration $[M^-]$ stays constant because we have assumed a zero diffusion coefficient for this species.

From Fig. 3, *g–l*, we can demonstrate that for an axon of this geometry, the membrane and the axial ion fluxes are equally important. In thinner axons, it may be expected that the membrane flux becomes more important because it scales with r_i as opposed to r_i^2 for the axial flux. The axial sodium flux is consistently inward because both the concentration and the voltage gradients force the sodium ions in this direction. This is not the case for potassium and chloride, for which a more complicated interaction between the axial gradients occurs. The membrane flux for sodium is consistently inward, whereas potassium moves in the opposite direction, as expected. The chloride membrane flux is one order of magnitude smaller than the sodium or potassium flux,

TABLE 1 **Parameters for the diffusion model**

Parameter	Description	Value	Comments
$[Na]_e$	Extracellular sodium concentration	425 mM	From Gilbert et al. (18)
$[K]_e$	Extracellular potassium concentration	10 mM	From Gilbert et al. (18)
$[Cl]_e$	Extracellular chloride concentration	555 mM	From Gilbert et al. (18)
$[C^{2+}]_e$	Extracellular cation concentration	60 mM	From Gilbert et al. (18)
$[A^-]_e$	Extracellular anion concentration	0 mM	From Gilbert et al. (18)
$[M^-]_e$	Extracellular protein concentration	0 mM	From Gilbert et al. (18)
$[Na]_i$	Intracellular sodium concentration	59 mM	From HH Nernst potential
$[K]_i$	Intracellular potassium concentration	207 mM	From HH Nernst potential
$[Cl]_i$	Intracellular chloride concentration	65 mM	From HH Nernst potential
$[C^{2+}]_i$	Intracellular cation concentration	0 mM	From Gilbert et al. (18)
$[A^-]_i$	Intracellular anion concentration	18 mM	From Gilbert et al. (18)
$[M^-]_i$	Intracellular protein concentration	183 mM	From electroneutrality
r_i	Axon radius	200.000 μm	Typical value
r_p	Outer radius periaxonal space	200.012 μm	From Adelman et al. (13)
r_s	Outer radius Schwann cell layer	200.920 μm	From Adelman et al. (13)
r_e	Bath radius	1,000.000 μm	Typical value
$f_{Schwann}$	Effective surface area of Schwann cell layer	1.05×10^{-3}	From Adelman et al. (13)
T	Temperature	295 K	Room temperature
D_{Na^+}	Sodium diffusion coefficient	1.24×10^{-9} m^2/s	From Robinson and Stokes (30)
D_{K^+}	Potassium diffusion coefficient	1.83×10^{-9} m^2/s	From Robinson and Stokes (30)
D_{Cl^-}	Chloride diffusion coefficient	1.90×10^{-9} m^2/s	From Robinson and Stokes (30)
D_{A^-}	Anion diffusion coefficient	1.24×10^{-9} m^2/s	Average for several anions
$D_{Ca^{2+}}$	Cation diffusion coefficient	1.53×10^{-9} m^2/s	Average for Mg^{++} and Ca^{++}
D_{M^-}	Protein diffusion coefficient	0 m^2/s	From Blum et al. (14)
C_m	Membrane capacitance	1 μF/cm^2	From Hodgkin and Huxley (1)
g_{Na}	Maximum sodium membrane permeability	1,200 S/m^2	From Hodgkin and Huxley (1)
g_K	Maximum potassium membrane permeability	360 S/m^2	From Hodgkin and Huxley (1)
g_{Cl}	Maximum chloride membrane permeability	3 S/m^2	From Hodgkin and Huxley (1)
g_{NaK}	Pump membrane conductivity	0.07 S/m^2	From Rakowski et al. (4)
V_{NaK}	Pump reversal potential	−220 mV	From Rakowski et al. (4)

which means that most of the chloride enters the axon through the cut. This explains the relatively slow progression of the chloride concentration profile in Fig. 3 *c* compared with potassium, for example.

At first glance, one might expect that the depolarized part of the axon would trigger action potentials continuously, but our calculations showed that this was not the case. The reason that the axon remains in a quasistatic state is that the membrane potassium conductance is greatly increased, even at slightly depolarized levels. Any

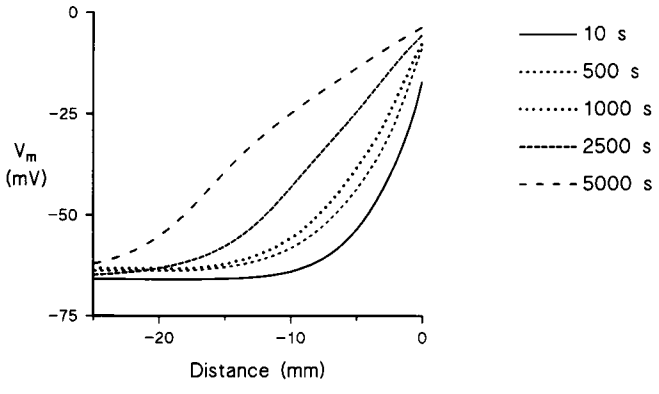

FIGURE 2 The resting membrane potential of a crushed, nonsealing squid giant axon as a function of the distance from the crush, located at 0.0 mm, at five different times after crushing.

inflow of charge due to sodium that might start an action potential is largely shunted by the potassium conductance, thereby reducing the net charge available for depolarizing the membrane. To verify this, we performed a separate calculation in which only a small, space-clamped patch of membrane was simulated. If the membrane was held at any voltage above the resting potential and the sodium and potassium gates were allowed to settle at the values associated with this potential, the axon immediately began to repolarize when the holding potential was removed, i.e., no action potential was elicited as a result of the depolarization.

Although the membrane potential changes only slowly after the initial profile is established, considerable electric currents flow for some time, as indicated in Fig. 4. The axial current flows continuously from the injury site into the axon and is initially as large as 6 μA for a 200-μm radius axon. This would quickly depolarize the axon were it not for the charge that disappears through the membrane (Fig. 4 *b*). However, the charge entering the axon is mostly carried by sodium, whereas the outflowing charge through the membrane consists mostly of potassium. Although it may take very little charge to depolarize the axon completely, it takes considerably more charge movement to exhaust the battery that is formed by the concentration differences between the intra- and extracellular space. A comparison between the

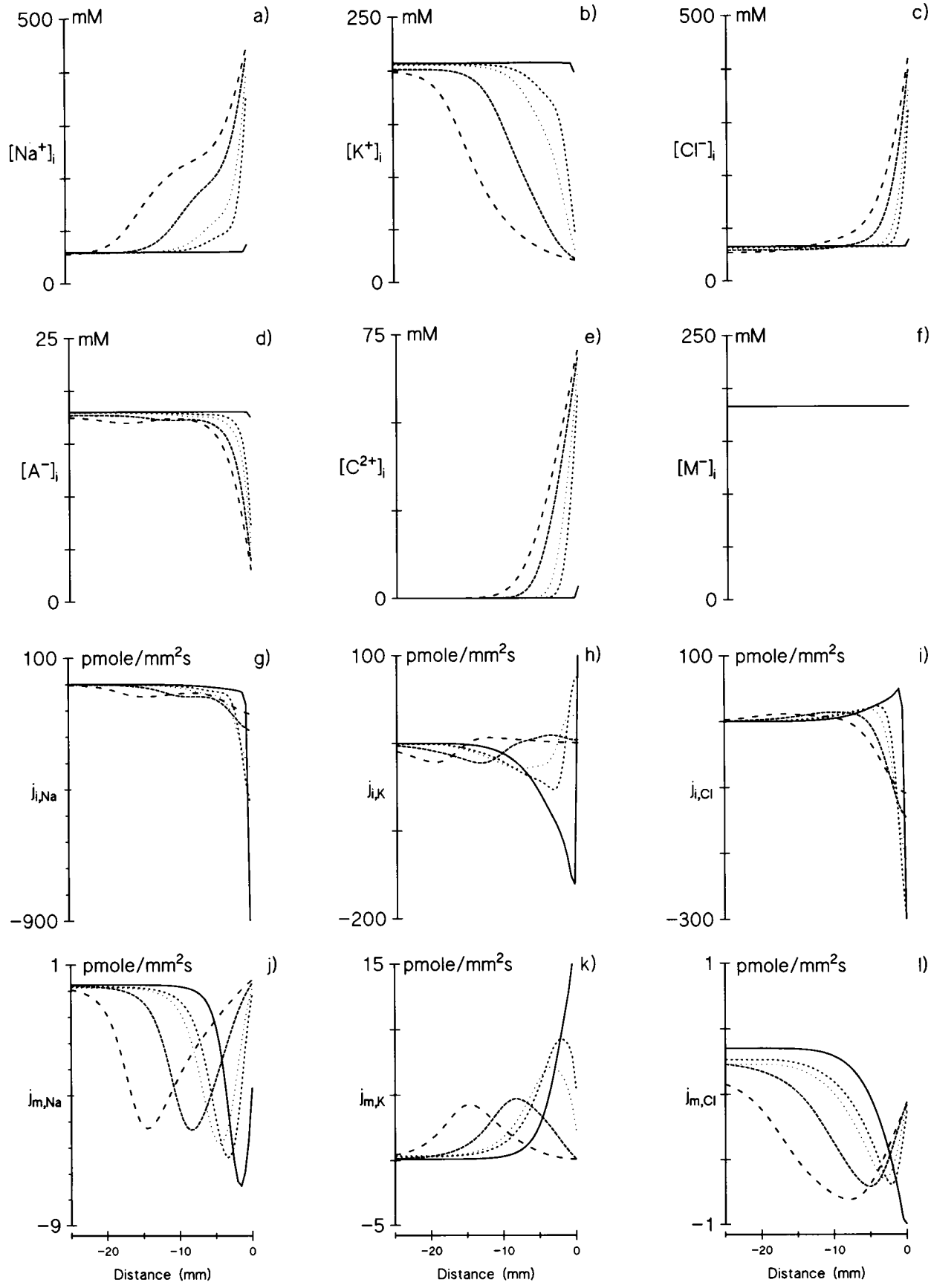

FIGURE 3 The intracellular ion concentrations [s] and axial, intracellular ion fluxes j_i, and the membrane ion fluxes j_m for a nonsealing squid giant axon as a function of the distance from the crush for five different times after crushing ranging from 10 to 5,000 s (for legend see Fig. 2).

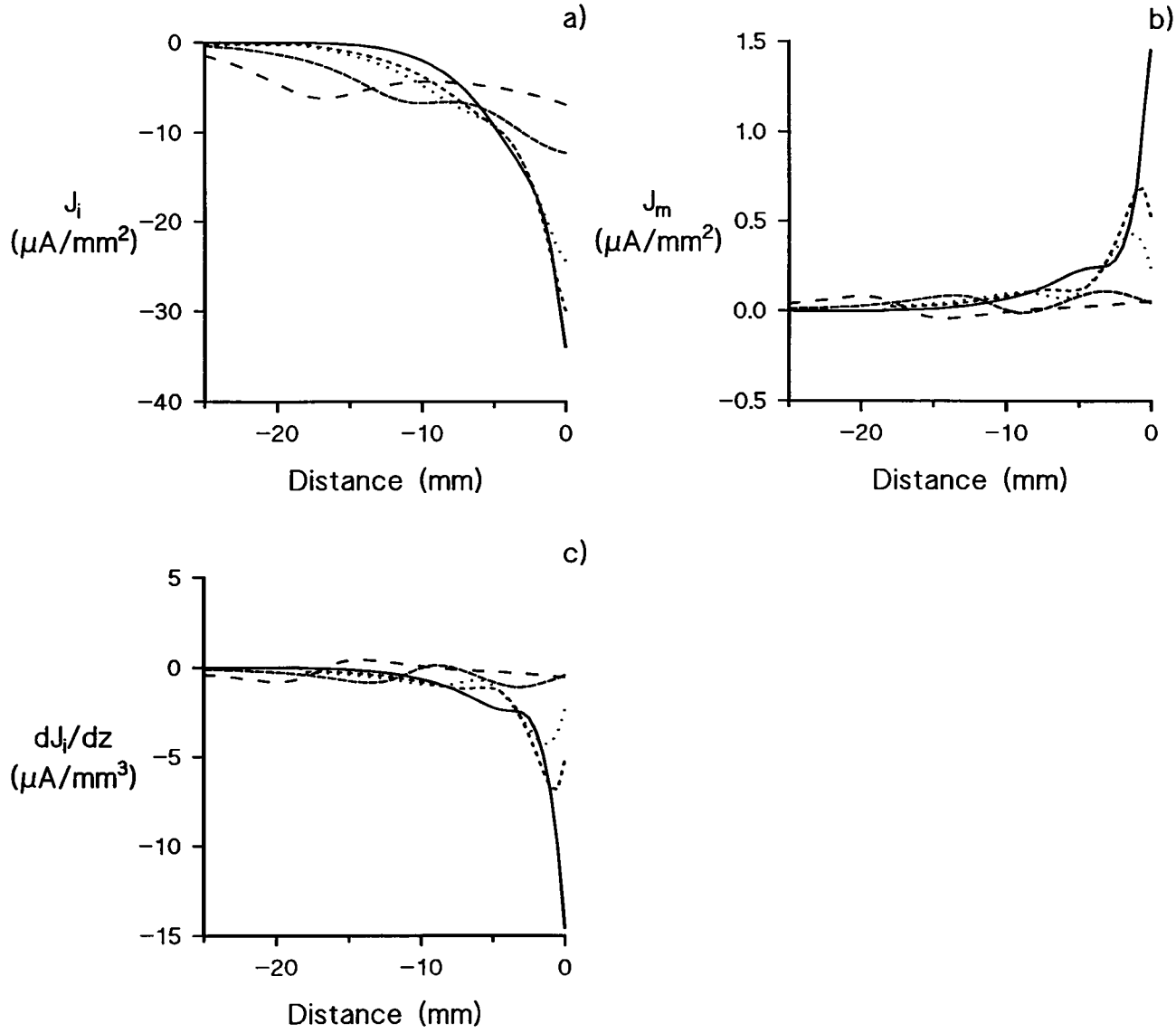

FIGURE 4 (*a*) The axial electric current density J_i in the nonsealing, crushed squid giant axon as a function of the distance from the crush for five different times after crushing (for legend see Fig. 2). The membrane current density J_m (*b*) and the spatial derivative of the axial current density (*c*) cancel each other almost completely so that the membrane potential changes only slowly.

gradient of the axial current (Fig. 4 *c*) and the membrane current density shows that the two virtually cancel each other, which results in a very slowly changing membrane potential.

The fact that the concentration battery stores a considerable amount of energy is demonstrated once more in Fig. 5 *a* with a plot of the axial injury current as a function of time at several positions, proximal to the cut. The time axes are logarithmic to show the early events more clearly. At the cut (*solid line*), the initial current density is $-45\ \mu A/mm^2$, but even 5,000 s after transection it still amounts to about $-7\ \mu A/mm^2$. At the cut, the current is strongest at the time of transection, but at some distance from the cut, the extremum occurs later: approximately 0.5 h after transection at a distance of 8 mm from the cut. As pointed out earlier, most of the inflowing charge is leaving the axon again as a membrane current density J_m, which is shown as a function of time in Fig. 5 *b*. The effect of inactivation becomes evident from the membrane current density at $z = 0$ mm. The outward membrane current, carried mostly by potassium, drops considerably in the first 10 s after transection, after which it decreases at a slower pace. This is a result of the closing of n_0. At more distant locations from the cut, this effect is not observed because the membrane depolarization is not as large in these regions (5).

Transected axons with sealing

In the literature, there are several reports of the sealing of nerve injuries (19–22). Some studies depend entirely on a visual inspection of the preparation (20), whereas others include multiple microelectrode measurements

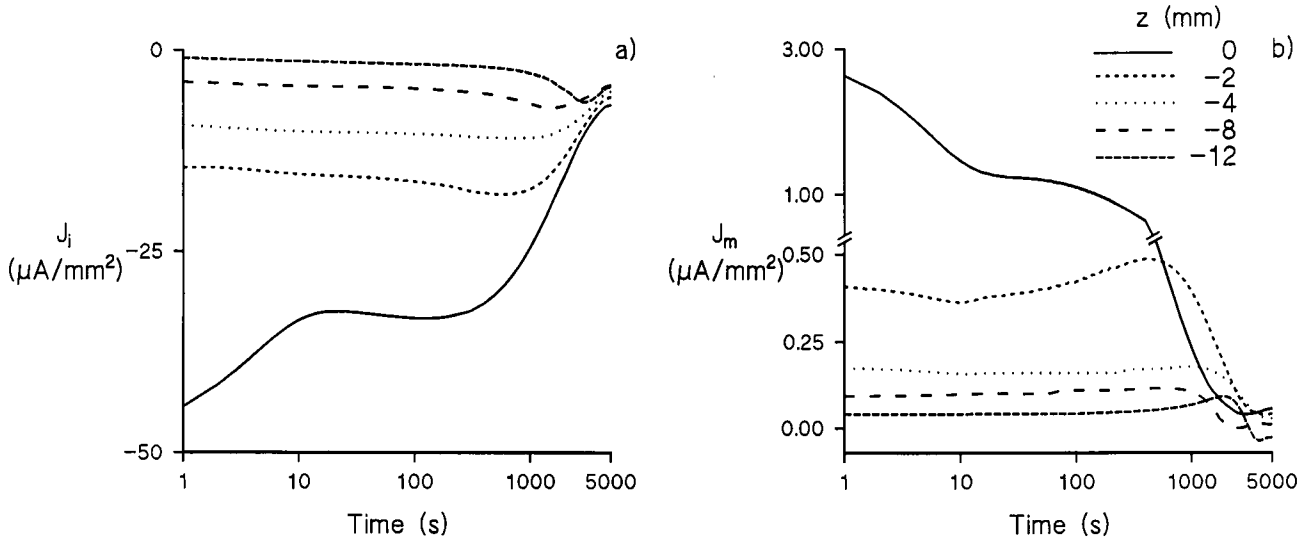

FIGURE 5 The axial injury current density J_i (a) and the membrane current density J_m (b) as a function of time for five different positions along the axon. The axon cross-sectional area is 0.126 mm^2.

(22). The seal appears at the injury site and consists of membrane-like material transported in small spherical vesicles called axosomes (19). At the opening, they form a diffusion barrier and may eventually isolate the axoplasm completely from the extracellular space, providing the first necessary step for regeneration. Ideally, one would track the progression of the intracellular voltage or concentration profiles to assess whether sealing is occurring, but this requires multiple long-term microelectrode recordings, which would be hampered by any significant voltage drift in the instrumentation or damage to the membrane at the site of microelectrode penetration. An alternative method is presented by van Egeraat et al. (21) where the axon is scanned with a biomagnetic current probe that does not require physical contact with the preparation (23–26). The probe measures the intracellular action currents associated with action signals that propagate into the injured region. Because the measurements are noninvasive, it is possible to obtain detailed profiles of the nonuniform electrical activity along the axon. The changes of these profiles with time can be compared with the model presented here to allow quantitative measurement of the sealing process.

Although it is known that sealing depends strongly on the presence of divalent cations in the extracellular space (22), there is not enough quantitative data available to propose a mechanism that can be included explicitly in the model. Therefore, the sealing is modeled as an independent closing of the open end that proceeds exponentially with time, with a time constant τ_{seal}. In this context, the nonsealing calculations discussed earlier correspond to τ_{seal} approaching infinity. We assume for now that no additional recovery mechanisms, such as increased active ion transport, will develop.

A series of model calculations predicts that there exists a critical value of the sealing time constant above which sealing is no longer effective. If the sealing does not take place soon after the injury, then a large enough region of the membrane becomes permanently depolarized to drive the further depolarization of the remaining axon. The membrane flux in the large depolarized region, consisting of incoming sodium and outflowing potassium, provides a sufficient number of ions to maintain this process. For the axon that we have modeled, this critical sealing time constant is ~135 s. This point is illustrated in Fig. 6, which shows the voltage profiles for a simulation with τ_{seal} equal to 100 s and one with a sealing time constant of 200 s. In the first case, the voltage profile steadily drops toward the normal resting potential of −65 mV. In the second case, however, the voltage profile shows the same qualitative effect, after some delay, as in the nonsealing case, in spite of the fact that at the time of the last profile (5 ks) the opening is virtually closed; the ion flow is sustained by the depolarized membrane.

Active ion transport and sealing

At this point it is worth discussing the role of active ion transport. In Fig. 3, a and b, the sodium and potassium concentrations stay relatively constant far from the cut, due to the sodium–potassium pump in our model. The intracellular sodium concentration (Fig. 3 a) even decreases slightly, which indicates that the 3:2 sodium–potassium pump has an overcapacity for sodium at this potential. However, some sodium may be used for secondary sodium driven pumps that could not be included in this model due to the lack of quantitative information. The same lack of reliable data prompted us to omit active chloride transport, which explains why the chloride concentration in Fig. 3 c displays a slow downward drift. Over the timespan considered in this simulation, active ion transport does not at first seem to play a major role. For example, the sodium pump current density in this

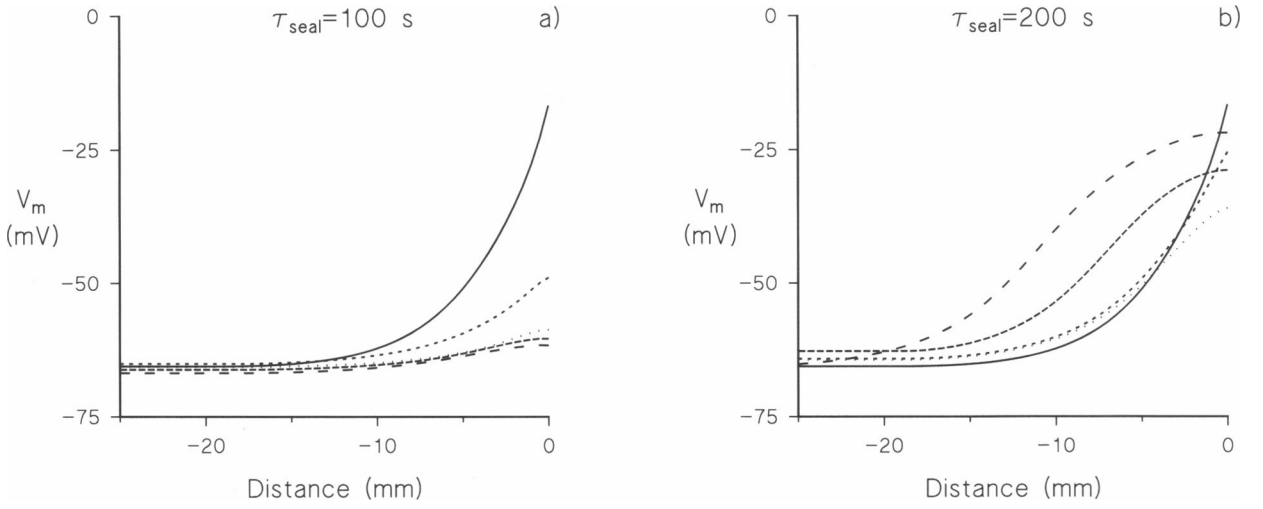

FIGURE 6 The membrane potential in a sealing, crushed squid giant axon for two different sealing time constants τ_{seal} at five different times. Notice in *b* that even though the axon is sealing, the depolarization continues to progress to the left even 5,000 s after crushing, when the seal is virtually complete (for legend see Fig. 2).

simulation does not exceed 0.45 pmol/mm^2 s, which is considerably lower than the total quasistatic sodium membrane flux in Fig. 3 *j* and also much less than the peak sodium influx during an action potential, which is on the order of 100 pmol/mm^2 s. However small the absolute contribution of active transport to the total ion movement, the effect of active transport is clearly noticeable in the critical sealing times. We repeated the simulation of a sealing axon without the 3:2 sodium–potassium pump and found that the critical sealing time constant was reduced to only 85 s. Therefore, active transport may play a crucial role in helping the axon survive the first few minutes after injury.

Sealing and channel inactivation

To study the effect of sodium channel inactivation and/or additional sodium membrane leakage, a parameter was added to the simulation model with a sealing time constant of 100 s. This parameter introduced a small sodium-specific membrane leak expressed as a percentage of the maximum sodium membrane permeability $\mathbf{g}_{Na}$ (see Table 1). As described before, this model sealed without the additional sodium leak. However, with a leak as small as 0.02%, sealing was no longer possible with a sealing time constant of 100 s. Larger leaks on the order of 0.1% yielded totally unrealistic simulation results where the membrane depolarized, even in the absence of a transection. Therefore, we conclude that sodium inactivation must be virtually complete as conceived in the original Hodgkin–Huxley model, where the steady-state sodium membrane permeability at the resting potential, given by the function m^3h is also on the order of 0.01%.

Potassium inactivation is included in our model through the inactivation gate n_0. Normally, n_0 varies between 0.2 and unity, according to the literature (5). When the membrane potential, V_m, is held constant for a time on the order of 1 min, n_0 slowly reaches a steady-state value that depends sigmoidally on V_m. For V_m at the resting potential of −65 mV, n_0 is close to unity. For membrane potentials of −40 mV or even more depolarized, n_0 approaches the value of 0.2. The monotonic transition of n_0 from unity to 0.2 takes place for V_m between −50 and −40 mV. The role of inactivation was studied by replacing n_0 in Eq. 8 by $k(n_0 - 1) + 1$, where k is a factor that varies the role of n_0 on the potassium membrane permeability. When k is 0, inactivation is basically removed from the model, whereas a value of unity yields our standard model. We studied the effect of this variation in a model with a sealing time constant set at 170 s, 35 s higher than the critical sealing time constant of 135 s of our standard model described earlier. This value was chosen in analogy with the study of sodium inactivation where we used a model with a 100-s sealing time constant; just as the lack of sodium inactivation is expected to shorten the critical sealing time, the lack of potassium inactivation is expected to prolong it. A larger potassium membrane conductance makes U_m in our model more negative and thus contributes to a faster repolarization of the membrane. Even in the extreme case when k was 0 (no inactivation), this axon did not seal, although the depolarization profiles as compared with Figs. 2 and 6 *b* were delayed in time; e.g., the 5 *ks* membrane potential profile of this simulation coincided approximately with the 2.5 *ks* profile of Fig. 6 *b*. At first glance this seemed unexpected, but a more careful analysis showed that relative magnitudes of the membrane permeabilities of sodium and potassium for membrane potentials between −60 and −50 mV are extremely important for the final result: either a steady return to the resting potential or an ongoing permanent depolarization. As discussed before, the steady-state value of n_0 is

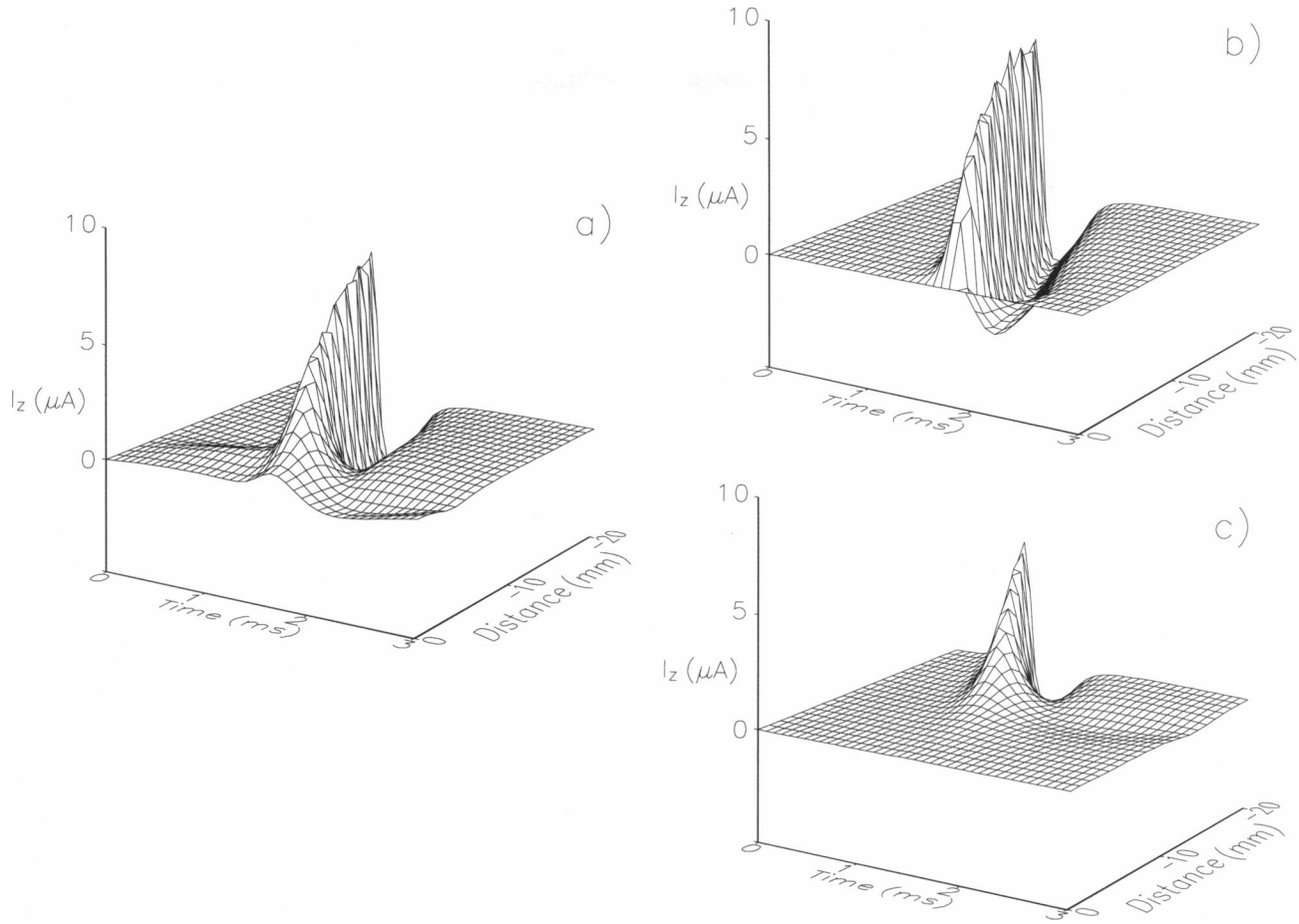

FIGURE 7 The action currents in a crushed squid giant axon as would be recorded with a magnetic current probe. The axon is stimulated at −32 mm from the crush, and the propagation of the action current is visualized as a function of space and time. (*a*) Simulation at 10 s after crushing. (*b*) At 1 h after crushing with τ_{seal} = 100 s. (*c*) At 1 h after crushing with no sealing.

still close to unity for membrane potentials in this range, so that inactivation does not play as large a role at a more depolarized membrane potential, e.g., −40 mV, where n_0 is 0.2.

Magnetic measurements of action currents

We have simulated a scan of the injured axon with the toroid. In this experiment, the axon is again stimulated at a point 32 mm from the cut. The action signal propagates toward the injured region but comes to a halt at a distance from the cut that depends on the time after transection and the degree of sealing. The first simulation (Fig. 7 *a*) is for both the sealing and nonsealing axons and represents a measurement 10 s after transection. The amplitude of the biphasic action current begins to drop 20 mm from the cut, and the decrease is stronger for the second phase amplitude than for the first, which turns the action current into an almost monophasic signal at 2–3 mm from the cut. The second graph (Fig. 7 *b*) is for the sealing axon with τ_{seal} = 100 s, and it gives the action current as it would appear, 1 h after transection. The action current propagates right up to the injury site and remains approximately biphasic. The third case is for a nonsealing axon with infinite τ_{seal} (Fig. 7 *c*). Propagation stops at 10–15 mm from the cut, which indicates that a considerable part of the axon has become permanently depolarized. This figure shows that the Biomagnetic Current Probe could readily distinguish the sealed and nonsealed case, and it also may be possible to determine the sealing time.

DISCUSSION

Our diffusion model can be used to simulate a variety of interesting physiological problems. In the present application, the nerve transection, we did not take advantage of the model's capability to represent systems with a restricted extracellular space. The bath radius was chosen 50 times larger than the axon radius, which means that the bath volume is ~2,500 times larger than the axoplasmic volume. This corresponds to a situation that is encountered in many experiments (19). The simulation of a transected axon requires the calculation of the concentration changes. A constant-concentration core conductor model could only reproduce the situation just after

transection, although a significant error would be made by omitting the liquid junction potentials. Once sealing has occurred in such a model, the action signals would be identical to the action signals propagating into a terminated fiber that was never injured. Ultimately, the time-course of sealing would not have an effect, which does not seem very realistic. In our variable-concentration model, the liquid junction potentials improve the accuracy as compared with constant-concentration models.

An interesting finding concerning the sealing is the critical time course. If sealing does not occur soon enough after the injury, then the membrane fluxes in the permanently depolarized part of the axon can sustain a further depolarization of the remaining part. This problem is expected to be even more important in smaller axons, where the ratio of intracellular volume to membrane area is smaller. If no additional recovery mechanisms, such as greatly increased active ion transport, are present, then significant sealing must occur within minutes or the process becomes irreversible.

Our model calculations predict that the axon is very sensitive to sodium inactivation or rather the lack of inactivation. To obtain realistic results with our model, the sodium permeability at rest must be $\ll 0.1\%$ of the maximum permeability. An even lower value for the upper limit may be determined when we compare experimental results of transected squid giant axons with our simulations. For potassium, the effect of inactivation is not as dramatic. An important reason is that the potassium inactivation is normally incomplete. This allows the influx of charge through the cut to be shunted largely to the bath. If potassium inactivation were to be more complete, then we expect that the axial current at the cut would continuously trigger action potentials, thereby exhausting the axon even quicker.

The sealed and unsealed case can be distinguished readily with a magnetic current probe measurement, as shown by van Egeraat et al. (21). The advantage of this technique is that it requires no physical contact between the probe and the preparation, thereby reducing the risk of additional injury or hampering of the sealing process.

Our analysis has pointed out possible inconsistency in the values of intracellular conductivity in the squid axon. If we use Eq. 3 and Table 1 to calculate the squid intracellular conductivity, then we obtain a value of 2.3 S/m, which is 20% lower than what Hodgkin and Huxley found (1) but probably within the range of error. However, if we use the ion activities (12) with an activity coefficient of 0.7 instead of the ion concentrations, the theoretical conductivity ends up around 1.6 S/m, which would lead to an even larger discrepancy between theory and experiment. The activity coefficient of 0.7 is given for a 200-mM KCl solution (12), which is a rough approximation of the axoplasmic composition. Possible explanations for this discrepancy include the activity coefficient being higher than expected or the presence of additional, mobile intracellular ions that would increase the conductivity. It is also possible that the intracellular concentrations reported in the literature are in fact the intracellular activities, but this is not clear. This would mean that the ion concentrations are actually higher than assumed but that part of the ion population does not participate in the electric behavior of the solution. In our calculations, we have assumed an activity coefficient of unity, which makes the activities equal to the concentrations.

The predictions of our model could be tested readily in a squid experimental preparation, where we can perform the measurements corresponding to Fig. 7. A direct measurement of the steady injury currents would be possible with a Superconducting QUantum Interference Device (SQUID) magnetometer (27). The magnitude of the injury current is large enough to produce a detectable magnetic field. A possible problem may be the spatial distribution of the current in a real experimental situation with a volume conductor. Most of the current that enters the axon through the cut leaves the axon again through the membrane within a few millimeters from the cut, creating current loops of detectable dipole moment but with a spatial extent that is smaller than can be resolved with most SQUID magnetometers used in magnetoencephalography, which have in general an absolute field sensitivity of better than 10 $fT/Hz^{1/2}$ but a spatial resolution on the order of centimeters. An instrument such as MicroSQUID (28) with a sensitivity of 100 $fT/Hz^{1/2}$ and 1-mm imaging resolution should be able to perform these measurements. Inspection of Fig. 4, for example, reveals that the injury current 8 mm from the cut after 1,000 s has a value of -7 μA that, at a 3-mm radius, produces a magnetic field of 470 pT, which could easily be detected by MicroSQUID.

Slowly varying currents such as demonstrated for injured nerves could act as the source of steady magnetic fields measured at the surface of the human body (29). Less severe pathological conditions or normal processes such as tissue growth also may exhibit concentration gradients that produce current loops. Magnetic detectors can be used to investigate these processes, but, as indicated before, the spatial resolution of these instruments should be an important consideration.

We are grateful for the valuable comments of John Barach.

This research was supported by National Institutes of Health grant NS 19794.

Received for publication 18 July 1991 and in final form 1 November 1992

REFERENCES

1. Hodgkin, A., and A. F. Huxley. 1952. A quantitative description of membrane current and its application to conduction and excitation in nerve. *J. Physiol. (Lond.)*. 117:500–544.
2. DiFrancesco, D., and D. Noble. 1985. A model of cardiac electri-

cal activity incorporating ionic pumps and concentration changes. *Philos. Trans. R. Soc. Lond. B Biol. Sci.* 307:353–398.

3. Bockris, J. O'M., and A. K. N. Reddy. 1972. Modern Electrochemistry. Vol. I. Plenum Press, New York. 1432 pp.
4. Rakowski, R. F., D. C. Gadsby, and P. De Weer. 1989. Stoichiometry and voltage dependence of the sodium pump in voltage-clamped, internally dialyzed squid giant axon. *J. Gen. Physiol.* 93:903–941.
5. Clay, J. R. 1989. Slow inactivation and reactivation of the K^+ channel in squid axons. *Biophys. J.* 55:407–414.
6. Gilly, W. M., and C. M. Armstrong. 1984. Threshold channels—a novel type of sodium channel in squid giant axon. *Nature (Lond.)*. 309:448–450.
7. Orkand, R. K., J. G. Nicholls, and S. W. Kuffler. 1966. Effect of nerve impulses on the membrane potential of glial cells in the central nervous system of amphibia. *J. Neurophysiol. (Bethesda)*. 29:788–806.
8. Trachtenberg, M. C., and D. A. Pollen. 1969. Neuroglia: biophysical properties and physiologic function. *Science (Wash. DC)*. 167:1248–1252.
9. Gardner-Medwin, A. R. 1981. Possible roles of vertebrate neuroglia in potassium dynamics, spreading depression and migraine. *J. Exp. Biol.* 95:111–127.
10. Kraig, R. P., and C. Nicholson. 1978. Extracellular ionic variations during spreading depression. *J. Neurosci.* 3:1045–1059.
11. Leão, A. A. P. 1944. Spreading depression of activity in the cerebral cortex. *J. Neurophysiol. (Bethesda)*. 7:359–390.
12. Plonsey, R. 1969. *Bioelectric Phenomena.* McGraw-Hill, New York. 305 pp.
13. Adelman, W. J., J. Moses, and R. V. Rice. 1977. An anatomical basis for the resistance and capacitance in series with the excitable membrane of the squid giant axon. *J. Neurocytol.* 6:621–646.
14. Blum, J., G. Lawler, M. Reed, and I. Shin. 1989. Effect of cytoskeletal geometry on intracellular diffusion. *Biophys. J.* 56:995–1005.
15. Chabala, L. D. 1984. The kinetics of recovery and development of potassium channel inactivation in perfused squid (*Loligo pealei*) giant axons. *J. Physiol. (Lond.)*. 356:193–220.
16. Ehrenstein, G., and D. L. Gilbert. 1966. Slow changes of potassium permeability in the squid giant axon. *Biophys. J.* 6:553–566.
17. Press, W. H., B. P. Flannery, S. A. Teukolsky, and W. T. Vetterling. 1989. Numerical Recipes in Pascal. Cambridge University Press, Cambridge, UK. 759 pp.
18. Gilbert, D. L., W. J. Adelman, Jr., and J. M. Arnold. 1990. Squid as Experimental Animals. Plenum Press, New York.
19. Fishman, H. M., K. P. Tewari, and P. G. Stein. 1990. Injury-induced vesiculation and membrane redistribution in squid giant axon. *Biochim. Biophys. Acta.* 1023:421–435.
20. Gallant, P. 1988. Effects of the external ions and metabolic poisoning on the constriction of the squid giant axon after axotomy. *J. Neurosci.* 8:1479–1484.
21. van Egeraat, J. M., R. Stasaski, J. P. Barach, R. N. Friedman, and J. P. Wikswo, Jr. 1993. The biomagnetic signature of a crushed axon: a comparison of theory and experiment. *Biophys. J.* 64:1299–1305.
22. Yawo, H., and M. Kuno. 1985. Calcium dependence of membrane sealing at the cut end of the cockroach giant axon. *J. Neurosci.* 5:1626–1632.
23. Barach, J. P., B. J. Roth, and J. P. Wikswo, Jr. 1985. Magnetic measurement of action currents in a single nerve axon: a core conductor model. *IEEE (Inst. Electr. Electron. Eng.) Trans. Biomed. Eng.* 32:136–140.
24. Gielen, F. L. H., B. J. Roth, and J. P. Wikswo, Jr. 1986. Capabilities of a toroid-amplifier system for magnetic measurement of current in biological tissue. *IEEE (Inst. Electr. Electron. Eng.) Trans. Biomed. Eng.* 33:910–921.
25. Roth, B. J., and J. P. Wikswo, Jr. 1985. The magnetic field of a single nerve axon: a comparison of theory and experiment. *Biophys. J.* 48:93–109.
26. Wikswo, J. P., Jr., J. P. Barach, and J. A. Freeman. 1980. Magnetic field of a nerve impulse: first measurements. *Science (Wash. DC)*. 208:53–55.
27. Wikswo, J. P., Jr., R. N. Friedman, A. W. Kilroy, J. M. van Egeraat, and D. S. Buchanan. 1990. Preliminary measurements with MicroSQUID. *In* Advances in Biomagnetism. S. J. Williamson, M. Hoke, G. Stroink, and M. Kotani, editors. Plenum, New York. 681–684.
28. Buchanan, D. S., D. B. Crum, D. Cox, and J. P. Wikswo, Jr. 1990. MicroSQUID: a close-spaced four channel magnetometer. *In* Advances in Biomagnetism. S. J. Williamson, M. Hoke, G. Stroink, and M. Kotani, editors. Plenum, New York. 677–679.
29. Cohen, D., Y. Palti, B. N. Cuffin, and S. J. Schmid. 1980. Magnetic fields produced by steady currents in the body. *Proc. Natl. Acad. Sci. USA.* 77:1447–1451.
30. Robinson, R. A., and R. H. Stokes. 1959. Electrolyte Solutions. Butterworth, London. 560 pp.